Transmitter Discovery through Radio-Visual Probabilistic Active Sensing

Luca Varotto
Department of Information Engineering
University of Padova, Italy
Email: luca.varotto.5@phd.unipd.it

Angelo Cenedese
Department of Information Engineering
University of Padova, Italy
Email: angelo.cenedese@unipd.it

Abstract—**Multi-modal Probabilistic Active Sensing (MMPAS) uses sensor fusion and probabilistic models to control the perception process of robotic sensing platforms. MMPAS is successfully employed in environmental exploration, collaborative mobile robotics, and target tracking, being fostered by the high performance guarantees on autonomous perception. In this context, we propose a bi-Radio-Visual PAS scheme (Ra^{2}ViPAS) to solve the transmitter discovery problem. Specifically, we firstly exploit the correlation between radio and visual measurements to learn a target detection model in a self-supervised manner. Then, the model is combined with antenna radiation anisotropies into a Bayesian Optimization framework that controls the platform. We show that the proposed algorithm attains an accuracy of 92%, overcoming two other probabilistic active sensing baselines.**

I. INTRODUCTION

Active sensing (AS) [1] consists in the control of a dynamical system with actuation and sensing capabilities (e.g., eye-in-hand manipulators [1]), with the purpose of automating the perception process and maximizing its efficiency. By leveraging the intimate interplay among estimation, perception, and control, AS stands at the nexus between automation and robotics research, fostered by the higher performance guarantees provided by actuated sensing platforms w.r.t passive counterparts [2]. Indeed, by enabling autonomous perception in robotics systems, AS is successfully employed in environmental exploration [3] collaborative mobile robotics [4] target tracking [5], and source seeking [6].

Along this line, *probabilistic* AS (PAS) [7] exploits incoming data to generate a belief map. This encodes the knowledge gathered during the sensing mission (e.g., target potential locations in tracking tasks [1]), and is used to guide the platform towards the next actions. More importantly, probabilistic approaches account for realistic perception uncertainties [8]; hence, they are suitable to manage real-world (noisy) scenarios, unmodeled dynamics, sensing nuisance. Furthermore, probabilistic decision making has high adaptivity properties [3], and it is useful when poor a-priori knowledge is available [9].

Novel technologies and the evolution in embedded systems have enabled the integration of different sensing modalities in autonomous robotic platforms, paving the way towards *multi-modal* PAS (i.e., MMPAS) [5]. The coupling of different information sources opens up new perspectives in scene perception: multi-sensor platforms enable parallelisation and spe-

cialisation [10], while sensors heterogeneity induces inherent robustness and complementarity (i.e., different properties of the environment can be perceived) [5]. Notably, the aggregated data allow inferences that are not possible with single-sensor measurements.

In this context, *Radio-Visual PAS* (RaViPAS) approaches have been recently designed to mitigate the inadequacies of camera and radio-only strategies [5], especially in localization tasks [11]. Indeed, the information richness of visual sensors may be impaired by occlusions and Field of View (FoV) directionality [11]. Radio frequency (RF) signals, instead, have wider ranges [12] and enable energy efficient localization from the extraction of the Received Signal Strength Indicator (RSSI) of standard packet traffic [12]. Furthermore, RF communication has low hardware requirements and comes as parasitic in many real-life scenarios, since most portable devices are WiFi or Bluetooth enabled. Nonetheless, environmental interference often limits the RF-based localization accuracy [12]. RaViPAS aims to combine the complementary benefits of RF signals with visual cues. The literature addressing radio-visual sensor fusion is still sparse and the RaViPAS framework is an open research field with methodological challenges and application opportunities: for example, energy-aware strategies are required to alternate the accurate but energy-harvesting camera measurements, with the rough but lighter radio observations [11], [13]. Furthermore, traditional RF-based solutions involve tiring human-labeled calibration processes [12]. In this regard, the integration of accurate camera measurements in self-supervised calibration methods have been proven to be beneficial [11], [13].

Contribution - In this work, we propose a RaViPAS scheme to solve the *transmitter discovery* problem hereafter described (Fig. 1), which, despite its apparent simplicity, remains a canonical problem in many application domains. A static radio-visual sensing platform is surrounded by targets whose number and location is initially unknown. Only one of them establishes communication with the platform through a radio transmitter (Tx) and the aim is to identify which target is the Tx. We design a Bayesian Optimization (BO) controller, leveraging the non-isotropic antenna radiation pattern at the receiver side. The exploration-exploitation trade off capabilities of BO are crucial for robust and efficient target localization [8]. In addition, RSSI-based localization techniques

hinging on BO [14], do not require any observation model. Hence, the tiring human-labeled calibration processes involved in traditional RF-based solutions can be avoided. To increase the robustness of the localization process, we include a target visual detectability model into the BO framework. To this aim, we devise a self-supervised training procedure, exploiting the correlation between radio-visual inputs. In this way, we automatize the dataset acquisition process and minimize human intervention. In accordance with PAS paradigm, the platform is guided by a probabilistic reward function, which is refined as new observations are collected. Numerical results show that the proposed algorithm overcomes a RF-only PAS scheme.

II. PROBLEM STATEMENT

Fig. 1 shows the main elements of the problem scenario, namely the targets and the sensing platform[1].

Sensing platform: The sensing platform is a static orientable smart camera [5], endowed with a real-time target detector [15] and two radio receivers [16].

The camera: Let $\mathcal{F}_0$ be the global reference frame, whose origin is centered in the platform position and whose axis Z_0 is orthogonal to the groundplane $\Pi \subset \mathbb{R}^2$ where the platform and the targets lie. We identify the platform state with its only degree of freedom, that is the camera pan angle (i.e., the orientation around Z_0)

$$s_t \in [-\pi, \pi], \quad t = LT_c, \ L \in \mathbb{N}, \tag{1}$$

where T_c is the camera frame rate. The camera pan angle defines the Field of View (FoV), $\Phi(s_t) \subset \Pi$, which is regulated through the control input u_t according to a deterministic Markovian transition model

$$s_{t+T_c} = s_t + u_t, \quad u_t \in [-\pi, \pi]. \tag{2}$$

The state transitions occur at multiple of $T > T_c$, namely

$$u_t = 0, \quad t \neq HT, \ H \in \mathbb{N}. \tag{3}$$

The receivers: The platform is endowed with two radio channels. The former, referred to as $\mathrm{Rx}^{(iso)}$, uses an omnidirectional antenna, while the latter, $\mathrm{Rx}^{(dir)}$, has a directional antenna [17]. The dominating lobe of $\mathrm{Rx}^{(dir)}$ is supposed to be aligned with the camera optical axis, but the knowledge on the overall radiation pattern of is inaccurate. We set

$$T = T_{\mathrm{RF}} = \nu T_c, \ \nu \in \mathbb{N}, \tag{4}$$

where T_{RF} is the sampling interval of both receivers. With the first equality ($T = T_{\mathrm{RF}}$), a control input is computed as a new RSSI sample is collected. The second equality ($T_{\mathrm{RF}} = \nu T_c$) is justified by the fact that radio reception has typically longer sample rates than cameras' acquisition [18].

[1]Bold letters indicate (column) vectors if lowercase, matrices otherwise. A Gaussian distribution over the random variable x with expectation μ and variance σ^2 is denoted as $\mathcal{N}(x|\mu, \sigma^2)$. A Bernoulli distribution with parameter p is denoted as $\mathcal{B}(p)$. The shorthand notation $z_{t_0:t_1}$ indicates a sequence $\{z_k\}_{k=t_0}^{t_1}$.
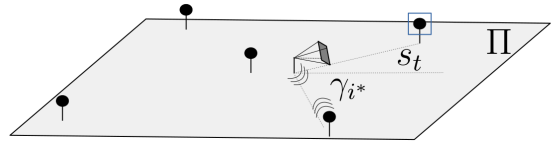

Fig. 1: Problem scenario. Five targets (black markers) surround the sensing platform; this communicates with one of the targets (Tx) through radio signals. The platform, at orientation s_t, detects a target (blue box). The Tx target can be detected when $s_t = \gamma_{i^*}$.

Targets: The platform is surrounded by N targets, which can be thought as people or marked objects, in civil or industrial settings. The targets are in Line-Of-Sight (LOS) w.r.t. the platform. The position of the i-th target w.r.t. $\mathcal{F}_0$ is denoted as $\mathbf{p}_i \in \Pi$. Accordingly, the distance of the i-th target to the platform is the Euclidean norm of $\mathbf{p}_i$ (i.e., $d_i = \|\mathbf{p}_i\|_2$). The number and the locations of the targets are unknown to the platform, but all N targets can be recognized through the camera object detector; moreover, one of the N targets establishes communication with the platform through an omnidirectional radio Tx. We denote with $i^* \in \{1, \dots, N\}$ the index of such target.

Perception modeling: Both platform receivers extract from received data packets the Received Signal Strength Indicator (RSSI), $r \in \mathbb{R}$. The RSSI is a measure of the received radio signal power [12] and it is theoretically related to the Tx-Rx distance d_{i^*} [12], namely

$$r^{(iso)} = g(d_{i^*}) \tag{5}$$

where $r^{(iso)}$ denotes the RSSI collected at $\mathrm{Rx}^{(iso)}$. To account for the non-isotropic pattern of the $\mathrm{Rx}^{(dir)}$, the relation (5) should be modified as

$$r_t^{(dir)} = g(d_{i^*})\varrho(s_t, \gamma_{i^*}), \ \varrho(s_t, \gamma_{i^*}) \in [0,1], \tag{6}$$

where γ_{i^*} is the angular position of Tx w.r.t $\mathcal{F}_0$, that is

$$\gamma_{i^*} = \arctan\left(\frac{p_{i^*, Y_0}}{p_{i^*, X_0}}\right) \tag{7}$$

with p_{i^*, X_0} and p_{i^*, Y_0} X_0 and Y_0 coordinates of $\mathbf{p}_{i^*}$, respectively. The function $\varrho(\cdot)$ is an attenuation factor that accounts for radiation pattern anisotropies through the misalignment of Tx and $\mathrm{Rx}^{(dir)}$. Indeed, the attenuation is minimal (i.e., $\varrho(s_t, \gamma_{i^*}) \approx 1$) if $s_t \approx \gamma_{i^*}$, that is, if Tx is along the axis of the dominating lobe. The attenuation increases together with the Tx-$\mathrm{Rx}^{(dir)}$ misalignment [17].

Motivated by the energy efficiency and the low-cost hardware requirements, RSSI-based localization systems have been widely studied in literature [5], [11]. Despite this, RSSI localization suffers from several drawbacks. At first, the functions $g(\cdot)$ and $\varrho(\cdot)$ are usually unknown and need to be estimated through extensive and time-consuming calibration procedures [12]. In this work, we propose a self-supervised methodology that requires minimal human intervention and does not need to estimate neither $g(\cdot)$, nor $\varrho(\cdot)$ (see Sec. III). A further limitation of RF-only localization systems resides on the high sensitivity to environmental interference (e.g., cluttering and multi-path distortions) [12]. Hence, the target

position is hidden in extremely noisy receiver measurements, according to the following *RSSI observation model*

$$z_{\text{RF},t} = r(\mathbf{p}_{i^*}) + v_{\text{RF},t}, \quad t = MT_{\text{RF}}, \ M \in \mathbb{N}$$
$$v_{\text{RF},t} \sim \mathcal{N}\left(v|0, \sigma_{\text{RF}}^2\right) \tag{8}$$

where $z_{\text{RF},t}$ is denoted either as $z_{\text{RF},t}^{(iso)}$ or $z_{\text{RF},t}^{(dir)}$, if $r(\mathbf{p}_{i^*})$ follows (5) or (6). A final issue of RSSI-based localization regards those techniques relying on omnidirectional receivers only [19]. As (5) highlights, the RSSI values are characterized by inherent ambiguities on the target position (i.e., they do not identify uniquely the position of the radio source). When the receiver is static, these ambiguities induce severe convergence issues in the estimation process [5]. For this reason, most literature solutions mitigate the ambiguity effects through multiple receivers [20], multi-modal (e.g., radio-visual) perception systems [5], or active sensing schemes [19].

As for the camera sensing capability, the visual detection process of target i is modeled as a Bernoulli random variable $D_t \in \{0,1\}$, with success probability [5]

$$p(D_t = 1|\mathbf{p}_i, s_t) = \begin{cases} p_D(d_i), & \text{if } \mathbf{p}_i \in \Phi(s_t) \\ 0, & \text{otherwise.} \end{cases} \tag{9}$$

As (9) highlights, the detection success probability is a function of both the camera orientation and the target-platform distance. In particular, visual depth effects [1] are accounted through $p_D(d_i)$, which is the *Probability of Detection* (POD) when the target is in FoV. In this work, we suppose that the same POD function can be applied to all targets, which is a reasonable assumption in most practical scenarios. If $i = i^*$, the dependence on d_i in (9) can be equivalently substituted by r_t, on the basis of (5).

Problem statement: The Tx discovery problem aims at identifying the Tx among the N targets. The LOS condition implies

$$\nexists(i,j) \text{ s.t. } \gamma_i = \gamma_j, \tag{10}$$

that is, each target is uniquely identified by its angular position w.r.t. the platform. Hence, the Tx discovery problem boils down to an *association* task on top of a uni-dimensional *localization* problem within a *noisy* scenario. The quantity to be estimated is the Tx angular position γ_{i^*}, assuming that the dynamics of the targets is slow w.r.t. the localization process. Formally, at time t, the result of the association task is

$$\hat{i}_t = \underset{i \in \{1,...,N\}}{\arg\min} |\hat{\gamma}_t - \gamma_i|, \tag{11}$$

where $\hat{\gamma}_t$ is the estimate of γ_{i^*} (i.e., the localization outcome).

III. METHODOLOGY

Indeed, the Tx discovery problem is ill-posed if tackled with passive strategies, due to the inherent RSSI ambiguities and the uncertainties on the receivers radiation pattern, and thus motivated, we propose an active sensing scheme.

Theoretically, the anisotropy of $\text{Rx}^{(dir)}$, coupled with the platform movements, provide sufficient information to reduce the RSSI ambiguities and solve the localization problem.
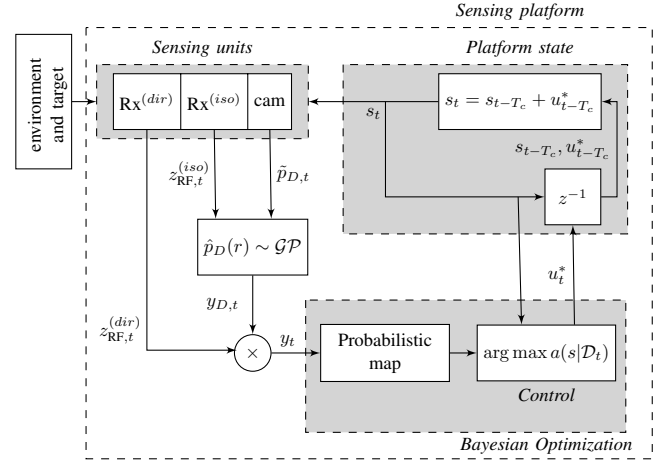

Fig. 2: Ra^{2}ViPAS scheme for the Tx discovery problem.

Nonetheless, in practical scenarios the noise in RSSI data affect the stability and reliability of RF-only strategies. Moreover, the lack of knowledge on the antenna radiation pattern often demands extensive calibration procedures. Therefore, we increase the localization robustness by combining radio and visual cues. Furthermore, we formulate the problem in a Bayesian probabilistic framework, which accounts for perception uncertainties and increases the adaptivity properties. Overall, we obtain the bi-Radio-Visual Probabilistic Active Sensing (Ra^{2}ViPAS) scheme depicted in Fig. 2 and detailed in the following. The Ra^{2}ViPAS is based on two steps:

1) first, we apply Gaussian Process Regression (GPR) to learn the function $p_D(r)$ in a self-supervised fashion (Sec. III-A);
2) then, we cast the localization task to a black-box optimization problem for which Bayesian Optimization (BO) is employed (Sec. III-B).

A. POD learning through GPR

GPR: A Gaussian Process (GP) is a collection of random variables, any finite number of which have a joint Gaussian distribution [21]. Given the input vector $\mathbf{x} \in \mathbb{R}^p$, a GP is fully specified by its mean function $m(\mathbf{x})$ and covariance function $k(\mathbf{x}, \mathbf{x}')$, namely

$$f(\mathbf{x}) \sim \mathcal{GP}\left(m(\mathbf{x}), k(\mathbf{x}, \mathbf{x}')\right), \tag{12}$$

where $f : \mathbb{R}^p \to \mathbb{R}$ is referred to as *latent function*. Mean and covariance (or kernel) functions incorporate prior knowledge (e.g., periodicity, smoothness) about the latent function. The mean function is typically constant (usually zero), while the most commonly-used kernel functions are constant, linear, square exponential or Matern, as well as compositions of multiple kernels [21]. The hyperparameters in the mean and covariance functions are computed by fitting the train dataset $\mathcal{D}$ of cardinality n_{train}

$$\mathcal{D} = \{(\mathbf{x}_j, y_j)\}_{j=1}^{n_{train}} = (\mathbf{X}, \mathbf{y})$$
$$\mathbf{X} = \begin{bmatrix} \mathbf{x}_1 & \dots & \mathbf{x}_{n_{train}} \end{bmatrix}^\top \in \mathbb{R}^{n_{train} \times p} \tag{13}$$
$$\mathbf{y} = \begin{bmatrix} y_1 & \dots & y_{n_{train}} \end{bmatrix}^\top \in \mathbb{R}^{n_{train}}.$$
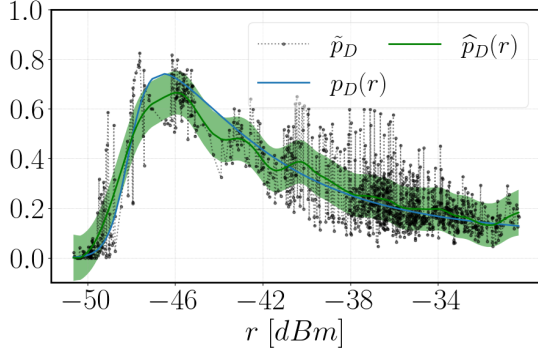
Fig. 3: Comparison between the latent function $p_D(r)$ (blue line) and the GP model $\widehat{p}_D(r)$ (green), learnt on the very noisy synthetic data $\{z_{\text{RF},i}^{(iso)}, \widetilde{p}_{D,i}\}_{i=1}^{n_{train}}$ (black markers).

Each training label y_j is a noisy measurement of the latent function $f(\mathbf{x})$, namely

$$y_j = f(\mathbf{x}_j) + \epsilon_j, \quad \epsilon_j \sim \mathcal{N}(\epsilon|0, \sigma^2). \tag{14}$$

To account for the i.i.d. Gaussian noise in the training labels, the GP in (12) becomes [21],

$$f(\mathbf{x}) \sim \mathcal{GP}\left(m(\mathbf{x}), k(\mathbf{x}, \mathbf{x}') + \sigma^2 \mathbf{I}\right). \tag{15}$$

This GP is used as *prior* for non-parametric Bayesian inference of the latent function. Consider the test inputs $\mathbf{X}_* = \begin{bmatrix} \mathbf{x}_{1,*} & \cdots & \mathbf{x}_{n_{test},*} \end{bmatrix}^\top \in \mathbb{R}^{n_{test} \times p}$. From the definition of a GP, any finite number of samples drawn from the GP are jointly Gaussian. Thus, according to [21],

$$\begin{bmatrix} \mathbf{y} \\ \mathbf{y}_* \end{bmatrix} = \mathcal{N}\left(\begin{bmatrix} \boldsymbol{\mu} \\ \boldsymbol{\mu}_* \end{bmatrix}, \begin{bmatrix} \mathbf{K}(\mathbf{X}, \mathbf{X}) + \sigma^2 \mathbf{I} & \mathbf{K}(\mathbf{X}, \mathbf{X}_*) \\ \mathbf{K}(\mathbf{X}_*, \mathbf{X}) & \mathbf{K}(\mathbf{X}_*, \mathbf{X}_*) \end{bmatrix}\right) \tag{16}$$

where: $\mathbf{y}_* = \begin{bmatrix} f(\mathbf{x}_{1,*}) & \cdots & f(\mathbf{x}_{n_{test},*}) \end{bmatrix}^\top \in \mathbb{R}^{n_{test}}$; the j-th row of $\boldsymbol{\mu}$ and $\boldsymbol{\mu}_*$ is $m(\mathbf{x}_j)$ and $m(\mathbf{x}_{j,*})$, respectively; the (i, k)-th entry of $\mathbf{K}(\mathbf{X}, \mathbf{X})$ and $\mathbf{K}(\mathbf{X}, \mathbf{X}_*)$ is $k(\mathbf{x}_j, \mathbf{x}_k)$ and $k(\mathbf{x}_j, \mathbf{x}_{k,*})$, respectively.

Making predictions about unobserved values $\mathbf{X}_*$ consists in drawing samples from the *predictive posterior distribution* of $\mathbf{y}_*$, given $\mathcal{D}$ and $\mathbf{X}_*$, that is

$$\begin{aligned} \mathbf{y}_*|\mathcal{D}, \mathbf{X}_* &\sim \mathcal{N}(\mathbf{y}_*|\boldsymbol{\mu}_{*|\mathcal{D}}, \boldsymbol{\Sigma}_{*|\mathcal{D}}) \\ \boldsymbol{\mu}_{*|\mathcal{D}} &= \boldsymbol{\mu}_* + \mathbf{K}(\mathbf{X}_*, \mathbf{X}) \left[\mathbf{K}(\mathbf{X}, \mathbf{X}) + \sigma^2 \mathbf{I}\right]^{-1} (\mathbf{y} - \boldsymbol{\mu}) \\ \boldsymbol{\Sigma}_{*|\mathcal{D}} &= \mathbf{K}(\mathbf{X}_*, \mathbf{X}_*) \\ &\quad - \mathbf{K}(\mathbf{X}_*, \mathbf{X}) \left[\mathbf{K}(\mathbf{X}, \mathbf{X}) + \sigma^2 \mathbf{I}\right] \mathbf{K}(\mathbf{X}, \mathbf{X}_*) \end{aligned} \tag{17}$$

POD learning through GPR: On the basis of (5), we consider the underlying POD as a function of the RSSI values and we model it as a GP, namely[2]

$$\widehat{p}_D(r) \sim \mathcal{GP}\left(0, k(r, r')\right). \tag{18}$$

The train dataset is

$$\mathcal{D} = \left\{ \left(z_{\text{RF},j}^{(iso)}, \widetilde{p}_{D,j} \right) \right\}_{j=1}^{n_{train}} \tag{19}$$

[2]The notation $\widehat{p}_D(r)$ is used to distinguish the GP model with the underlying POD, $p_D(r)$.

where the inputs are RSSI observations from $\text{Rx}^{(iso)}$ and the labels are the *empirical POD* between two RSSI samples, according to (4), that is

$$\widetilde{p}_{D,j} = \frac{1}{\nu} \sum_{\ell=1}^{\nu} D_{j,\ell}. \tag{20}$$

where $\{D_{j,\ell}\}_{\ell=1}^\nu$ are the ν detection outcomes before $z_{\text{RF},j}^{(iso)}$ is collected. Notably, $\mathcal{D}$ is automatically acquired by the platform (i.e., no human labeling is required[3]). If T_{RF} is sufficiently small w.r.t. the target movements, $\{D_{j,\ell}\}_{\ell=1}^\nu$ is a sequence of i.i.d. random variables with distribution $\mathcal{B}\left(p_D(r_j)\right)$, according to (5) and (9). Then, for a high frame rate camera [18], from the Central Limit Theorem, $\widetilde{p}_{D,j}$ converges in distribution to

$$\mathcal{N}\left(\widetilde{p}_{D,i} \,\middle|\, p_D(r_j), \frac{p_D(r_j)(1 - p_D(r_j))}{\nu}\right), \text{ as } \nu \to \infty. \tag{21}$$

Thus, the latent function is related to the noisy labels through the generative model

$$\begin{aligned} \widetilde{p}_{D,j} &= p_D(r_j) + \epsilon_j \\ \epsilon_j &\sim \mathcal{N}\left(\epsilon \,\middle|\, 0, \frac{p_D(r_j)(1 - p_D(r_j))}{\nu}\right), \end{aligned} \tag{22}$$

and the GPR problem is well-posed[4].

Fig. 3 shows an example of POD learning through GPR over synthetic data (see Sec. IV for the data generation process). The true POD function is

$$p_D(d) = \left[\left(1 + e^{4(d-4.5)}\right)\left(1 + e^{-(d-2.5)}\right)\right]^{-1}. \tag{23}$$

The GP model uses a zero mean function and a Matern covariance [21]. To evaluate the regression performance we use the coefficient of determination $R^2 \in (-\infty, 1]$

$$R^2 = 1 - \frac{\sum_{j=1}^{n_{train}} \left(p_D(r_j) - \widehat{p}_{D,*}(r_j)\right)^2}{\sum_{j=1}^{n_{train}} \left(p_D(r_j) - \frac{1}{n_{train}} \sum_{k=1}^{n_{train}} p_D(r_k)\right)^2} \tag{24}$$

where $\widehat{p}_{D,*}(r_j)$ is the POD prediction, according to (17). The higher R^2, the better the fit; in the case of Fig. 3, $R^2 = 0.94$.

B. Ra²ViPAS for Transmitter Discovery

The already introduced Fig. 2 shows the Ra²ViPAS pipeline. The information gathered by the platform sensing channels is aggregated and injected into a BO scheme. This exploits a GPR sub-module to reconstruct a probabilistic approximation of the localization objective function. This is then used to generate platform control inputs.

[3]To this aim, the camera and the receiver must be synchronized.

[4]As (22) highlights, the generative model of the labels is input-dependent (i.e., the GP is heteroscedastic [22]). Moreover, the GPR works on noisy inputs, according to (8). To deal with heteroscedasticity and noisy inputs, several ad-hoc methods have been proposed in literature [22].

BO: BO is a procedure designed for derivative-free global optimization, particularly suited for objective functions that are expensive to evaluate [23]. Formally, BO aims to solve the following optimization problem

$$\mathbf{x}^* = \arg\max_{\mathbf{x}\in\mathcal{X}} J(\mathbf{x}) \qquad (25)$$

where $\mathcal{X}$ is a domain space of interest; the objective function $J : \mathcal{X} \to \mathbb{R}$ is unknown (i.e., black-box optimization), but can be evaluated at any arbitrary query point $\mathbf{x}_* \in \mathcal{X}$. This evaluation produces a noise-corrupted (stochastic) output $y \in \mathbb{R}$. To solve (25), BO adopts a sequential procedure. At first, the objective function is approximated by a probabilistic model (e.g., a GP), easier to optimize and referred as surrogate function. The surrogate model is sequentially refined via Bayesian posterior updating (e.g., GPR), as new data are collected. To this aim, given the collected dataset $\mathcal{D}_t = \{(\mathbf{x}_j, y_j)\}_{j=1}^{t}$, the next query point is chosen according to a suitable selection criterion $a(\mathbf{x}|\mathcal{D}_t)$ (acquisition function)

$$\mathbf{x}_{t+1} = \arg\max_{\mathbf{x}\in\mathcal{X}} a(\mathbf{x}|\mathcal{D}_t). \qquad (26)$$

The acquisition function is designed over the surrogate function to balance exploration with exploitation, and to quantify the utility of a query point to produce a more informative posterior distribution. In this work, we have used the GP Upper Confidence Bound (UCB), namely

$$a(\mathbf{x}|\mathcal{D}_t) = \mu_{*,\mathcal{D}_t} + \sqrt{\beta}\sigma_{*,\mathcal{D}_t} \qquad (27)$$

where (17) is applied, $\sigma_{*,\mathcal{D}_t}$ is $\boldsymbol{\Sigma}_{*,\mathcal{D}_t}$ with $n_{test} = 1$, and β is an exploration-exploitation tuning hyperparameter.

Probabilistic Controller: The Tx location satisfies

$$\gamma_{i^*} = \arg\max_{\gamma\in[-\pi,\pi]} \underbrace{J_D(\gamma)J_{\mathrm{RF}}(\gamma)}_{J(\gamma)}$$
$$J_D(\gamma) = -|p(D|\mathbf{p}_{i^*}, \gamma_{i^*}) - p(D|\mathbf{p}_{i^*}, \gamma)| \qquad (28)$$
$$J_{\mathrm{RF}}(\gamma) = \varrho(\gamma, \gamma_{i^*}).$$

Specifically: the detectability term, $J_D(s)$, favors those values of γ where the target has the same (measured) POD of the Tx; on the other side, the RF term, $J_{\mathrm{RF}}(s)$, accounts for the radiation pattern and gives higher rewards when $\mathrm{Rx}^{(dir)}$ is aligned with Tx. The lack of precise knowledge on $\varrho(\cdot)$ makes (28) a black-box optimization problem; hence, it can be opportunely solved via BO. At time t, the dataset is

$$\mathcal{D}_t = \{(s_j, y_j)\}_{j=T_{\mathrm{RF}}}^{t} \qquad (29)$$

with $y_j = y_{D,j} y_{\mathrm{RF},j}$ and

$$y_{D,j} = -|\hat{p}_{D,*}(z_{\mathrm{RF},j}^{(iso)}) - \tilde{p}_{D,j}|$$
$$y_{\mathrm{RF},j} = |z_{\mathrm{RF},j}^{(dir)}|/\zeta, \qquad (30)$$

where ζ is a user-defined scaling hyper-parameter. Note that, $z_{\mathrm{RF},t}^{(dir)}/\zeta$ is a (noisy) scaled version of $J_{\mathrm{RF}}(\cdot)$, according to (8) and (6); however, this does not affect the optimization process, since the scale is $g(d_{i^*})$, which does not depend on s_t. Regarding $y_{D,t}$, it is a noisy version of $J_D(\cdot)$, where the noise comes from both the estimation error in $\hat{p}_{D,*}(z_{\mathrm{RF},t}^{(iso)})$

TABLE I: Setup parameters for the MC experiment.

Parameter	Value
T_{RF}	$0.1\,\mathrm{s}$
ν	10
n_{train}	900
n_{test}	120
N_{tests}	50
N	20
$f(d_t, \eta_t)$	$d_t + \eta_t \quad \eta_t \sim \mathcal{N}(0, 0.04)$
$g(d_{i^*})$	$\kappa - 10n\log_{10}(d_t/\delta) \quad \kappa = -30\,\mathrm{dBm},\ n=2,\ \delta=1\,\mathrm{m}$
$\varrho(s_t, \gamma_{i^*})$	$1 - 0.5(s_t - \gamma_{i^*})^2$
σ_{RF}	$3\,\mathrm{dBm}$
$p_D(d)$	$\left[\left(1 + e^{4(d-4.5)}\right)\left(1 + e^{-(d-2.5)}\right)\right]^{-1}$

and the measurements error in $\tilde{p}_{D,t}$ (see Sec. III-A). We use the dataset (29), to approximate $J(\gamma)$ via GPR (see Fig. 2). The GP model that approximates $J(\gamma)$ is the probabilistic map from which the next control input is computed

$$u_t = \begin{cases} \arg\max_{s\in[-\pi,\pi]} a(s|\mathcal{D}_t) - s_t, & t = HT_{\mathrm{RF}} \\ 0, & \text{otherwise,} \end{cases} \qquad (31)$$

where condition (3), with $T = T_{\mathrm{RF}}$, is taken into account. Finally, the estimate of γ_{i^*} at time t is the maximum of the GP predictive posterior mean (17), namely

$$\hat{\gamma}_t = \arg\max_{\gamma\in[-\pi,\pi]} \mu_{*|\mathcal{D}_t} \qquad (32)$$

IV. NUMERICAL RESULTS

To evaluate the proposed approach, we consider a Python-based synthetic environment[5]. Sec. IV-A describes the main setup parameters, as well as the synthetic data generation process. Sec. IV-B defines the metrics used for performance assessment and the baselines considered for comparison. The numerical simulation results are discussed in Sec. IV-C.

A. Setup parameters

To carry out realistic simulations, most parameters reflect real device characteristics. Tx and $\mathrm{Rx}^{(iso)}$ are supposed to be equipped with Nordic nRF52832 SoCs [16]; $\mathrm{Rx}^{(dir)}$ differs from $\mathrm{Rx}^{(iso)}$ in that the attenuation gain follows the function in Tab. I [17]. The function $g(\cdot)$ follows the log-distance Path Loss Model (PLM) with noise level $\sigma_{\mathrm{RF}} = 3\,\mathrm{dBm}$ [12]. The radio sampling time is set to $T_{\mathrm{RF}} = 0.1\,\mathrm{s}$, and the value of ν is set to 10, as a reasonable trade-off between typical real-life values and the ideal condition stated in (21). The underlying POD function is (23), designed according to real-life experiments [13]. During the POD learning phase, the target is supposed to move according to the stochastic linear model reported in Tab. I. Finally, we test the proposed approach in a crowded environment with $N = 20$ targets.

B. Performance assessment

To capture the performance variability, numerical evaluation is performed through a Monte Carlo (MC) experiment, composed by $N_{tests} = 50$ tests of duration $T_W = n_{test}T_{\mathrm{RF}}$ each, where $n_{test} = 120$ is the number of RSSI collected. At each MC test the position of the N targets is randomly chosen.

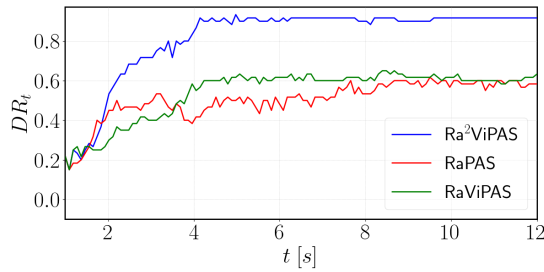[5]https://github.com/luca-varotto/Tx-discovery

Fig. 4: DR of Ra^{2}ViPAS, RaPAS and RaViPAS over a MC experiment.

Performance metric: The performance of the Tx discovery task is evaluated through the *Discovery Rate*

$$DR_t = \frac{1}{N_{tests}} \sum_{j=1}^{N_{tests}} \mathbb{1}_{\hat{i}_t = i^*}, \quad \mathbb{1}_{\hat{i}_t = i^*} = \begin{cases} 1, & \text{if } \hat{i}_t = i^* \\ 0, & \text{otherwise,} \end{cases} \quad (33)$$

where $\hat{i}_t$ follows (11). From a probabilistic perspective, DR_t is the empirical probability of identifying Tx at time t over the MC tests.

Baselines: The following original baselines are considered, all leveraging the main PAS approach proposed here:

- *RaPAS*: same pipeline of Ra^{2}ViPAS, but only Rx$^{(dir)}$ is used, namely $y_t = y_{RF,t}$.
- *RaViPAS*: same pipeline of Ra^{2}ViPAS, but Rx$^{(dir)}$ is not used, namely $y_t = y_{D,t}$.

C. Discussion

Fig. 4 depicts the discovery rate of Ra^{2}ViPAS, RaViPAS and RaPAS. The control law (31) induces the same qualitative behavior in all three algorithms, even though with different final results.

Initially, the sparse sampling of the search domain $[-\pi, \pi]$ produces wrong localization solutions (32); therefore, DR is low. At the same time, the sparse domain coverage implies large uncertainties in the surrogate model; this induces an explorative platform behavior, according to (27). BO generates an efficient exploration process that allows the platform to focus on regions that are more likely to optimize the objective function; hence, DR increases remarkably in this phase. When enough information is collected, exploitation overcomes exploration and DR meets a converge. Fig. 4 shows that Ra^{2}ViPAS has a short exploration phase (≈ 4 s) with the highest ($\approx 92\%$) and smoothest convergence behavior. This means that the information fusion process employed in Ra^{2}ViPAS produces a fast and efficient information gain, which leads to high estimation accuracy, stability and robustness.

In conclusion, the performance of Ra^{2}ViPAS justifies the higher hardware requirements w.r.t. RaPAS and RaViPAS.

V. CONCLUSION

This work proposes a probabilistic bi-radio-visual active sensing framework, applied to the transmitter discovery problem. We combine target visual detectability and radio signal strength into a Bayesian Optimization framework, responsible for the generation of the platform control movements. The approach can be extended to various application domains

and in the specifically considered scenario the suggested strategy attains a 92% accuracy level, 30% higher than the two baselines under comparison. Future work will be devoted to real-life experiments and to the extension of Ra^{2}ViPAS to cluttered dynamic contexts.

REFERENCES

[1] S. Radmard and E. A. Croft, "Active target search for high dimensional robotic systems," *Autonomous Robots, 41, 1, 163–180*, 2017.

[2] T. Patten, W. Martens, and R. Fitch, "Monte carlo planning for active object classification," *Autonomous Robots, 42, 2, 391–421*, 2018.

[3] M. Popovic, "Enviromental mapping and informative path planning for UAV-based active sensing," Ph.D. dissertation, ETH Zurich, 2019.

[4] P. Ghassemi and S. Chowdhury, "An extended bayesian optimization approach to decentralized swarm robotic search," *Journal of Computing and Information Science in Engineering*, vol. 20, no. 5, 2020.

[5] L. Varotto, A. Cenedese, and A. Cavallaro, "Probabilistic radio-visual active sensing for search and tracking," *arXiv:2011.10474*, 2020.

[6] M. Park and H. Oh, "Cooperative information-driven source search and estimation for multiple agents," *Inf. Fusion*, vol. 54, pp. 72–84, 2020.

[7] J. P. Queralta, J. Taipalmaa, B. C. Pullinen, V. K. Sarker, T. N. Gia, H. Tenhunen, M. Gabbouj, J. Raitoharju, and T. Westerlund, "Collaborative multi-robot systems for search and rescue: Coordination and perception," *arXiv preprint arXiv:2008.12610*, 2020.

[8] A. A. Meera, M. Popović, A. Millane, and R. Siegwart, "Obstacle-aware adaptive informative path planning for uav-based target search," in *2019 International Conference on Robotics and Automation (ICRA)*. IEEE, 2019, pp. 718–724.

[9] J.-P. Ramirez, E. A. Doucette, J. W. Curtis, and N. Gans, "Moving target acquisition through state uncertainty minimization," in *2014 American Control Conference*. IEEE, 2014, pp. 3425–3430.

[10] L. Esterle, P. R. Lewis, R. McBride, and X. Yao, "The future of camera networks: Staying smart in a chaotic world," in *Proc. of the 11th International Conf. on Distributed Smart Cameras*, 2017, pp. 163–168.

[11] A. de San Bernabé, J. Martinez-de Dios, and A. Ollero, "Efficient integration of rssi for tracking using wireless camera networks," *Information Fusion*, vol. 36, pp. 296–312, 2017.

[12] A. Zanella, "Best practice in rss measurements and ranging," *IEEE Communications Surveys & Tutorials, 18, 4, 2662–2686*, 2016.

[13] L. Varotto and A. Cenedese, "Probabilistic rf-assisted camera wake-up through self-supervised gaussian process regression," *arXiv preprint arXiv:2102.03350*, 2021.

[14] M. Carpin, S. Rosati, M. E. Khan, and B. Rimoldi, "Uavs using bayesian optimization to locate wifi devices," *arXiv preprint:1510.03592*, 2015.

[15] J. Redmon, S. Divvala, R. Girshick, and A. Farhadi, "You only look once: Unified, real-time object detection," in *Proc. of the IEEE conference on computer vision and pattern recognition*, 2016, pp. 779–788.

[16] N. Semiconductor. (2020) "nrf52832 technical reference manual". [Online]. Available: https://www.nordicsemi.com/-/media/Software-and-other-downloads/Product-Briefs/nRF52832-product-brief.pdf

[17] J. L. Gómez-Tornero, D. Cañete-Rebenaque, J. A. López-Pastor, and A. S. Martínez-Sala, "Hybrid analog-digital processing system for amplitude-monopulse rssi-based mimo wifi direction-of-arrival estimation," *IEEE Journal of Selected Topics in Signal Processing*, vol. 12, no. 3, pp. 529–540, 2018.

[18] M. Vollmer and K.-P. Möllmann, "High speed and slow motion: the technology of modern high speed cameras," *Physics Education*, vol. 46, no. 2, p. 191, 2011.

[19] S. A. A. Shahidian and H. Soltanizadeh, "Single-and multi-UAV trajectory control in RF source localization," *Arabian Journal for Science and Engineering*, vol. 42, no. 2, pp. 459–466, 2017.

[20] V. Cantón Paterna, A. Calveras Auge, J. Paradells Aspas, and M. A. Perez Bullones, "A bluetooth low energy indoor positioning system with channel diversity, weighted trilateration and kalman filtering," *Sensors*, vol. 17, no. 12, p. 2927, 2017.

[21] C. K. Williams and C. E. Rasmussen, *Gaussian processes for machine learning*. MIT press Cambridge, MA, 2006.

[22] A. McHutchon and C. Rasmussen, "Gaussian process training with input noise," *Advances in Neural Information Processing Systems*, vol. 24, pp. 1341–1349, 2011.

[23] P. I. Frazier, "A tutorial on bayesian optimization," *arXiv preprint arXiv:1807.02811*, 2018.